Investigation of High Efficiency GaAs Solar Cells

Larry C. Olsen, Glen Dunham, F.W. Addis, and Dan Huber
Tri-Cities University Center
Richland, WA

Kurt Linden
Spire Corporation
Bedford, MA

This paper concerns investigations of basic mechanisms which limit the performance of high efficiency GaAs solar cells. P/N heteroface structures have been fabricated from MOCVD epi-wafers. Typical AM1 efficiencies are in the 21–22% range, with a SERI measurement for one cell being 21.5%. The cells are nominally 1.5 × 1.5 cm in size. Studies have involved photoresponse, T–I–V analyses, and interpretation of data in terms of appropriate models to determine key cell parameters. Results of these studies are utilized to determine future approaches for increasing GaAs solar cell efficiencies.

Introduction

Electro-optical characteristics of high efficiency GaAs solar cells have been investigated in an effort to identify approaches to further improvement of cell performance. This work is part of an effort to optimize the GaAs cell structure for maximum efficiency. In the following sections, cell fabrication, performance, photoresponse analyses and current-voltage analyses are discussed.

Cell Fabrication and Performance

GaAs solar cell structures studied in this work were fabricated from epi-wafers purchased from Spire Corporation. Layered structures were grown by MOCVD according to our specifications. All other steps in cell fabrication were carried out at the Tri-Cities University Center (TUC).

The basic cell structure is described by Figure 1. An outline of cell fabrication procedures is given in Table 1. The features which distinguish the TUC approach are the use of electroplated Au and Au(Sn) contacts, $Al_xGa_{1-x}As$ back reflector with x = 0.45, and a 1.5 × 1.5 cm die size. The use of a P^+ GaAs cap layer, the emitter and base layer thicknesses are similar to those used by other groups.

Illuminated current-voltage characteristics measured by SERI are given in Figure 2. Numerous cells have been fabricated which exhibit an efficiency between 21% and 22%.

Photocurrent Analyses

A photon economy analysis has been carried out to identify approaches to increase the photocurrent of GaAs cells discussed in this paper. External photoresponse of cells was measured versus wavelength before AR coatings were deposited. Internal photoresponse was then determined by measuring the reflected photon flux and accounting for collector grid shadowing.

The internal photoresponse data were interpreted in terms of the electron band structure described by Figure 3. We have found that a single region emitter model is inadequate to fit the internal photoresponse data, even if the aluminum concentration of the AlGaAs window layer is allowed to vary. Photoresponse data are fit exceptionally well if two assumptions are made, namely: the window layer is assumed to have a x-value on the order of 0.65; and the emitter is assumed to have a dead region adjacent to the AlGaAs window layer. Referring to Figure 3, layer 3A is the dead layer, that is, the minority carrier lifetime is assumed to be zero in layer 3A. The two region emitter model used here is a limiting case. In particular, we assume that minority carrier transport in the emitter only takes place in layer 3B, with the interface between 3A and 3B being characterized by a surface recombination velocity S_F.

Assumed values for the optical absorption coefficient versus wavelength for $Al_xGa_{1-x}As$ are given in Figure 4. Presently, a complete set of experimental optical constants for all values of x does not exist. Semiempirical expressions for the absorption coefficient of $Al_xGa_{1-x}As$ were used which contained parameters used to fit data at the compositional ends of GaAs and AlAs This approach, with a few variations, was first employed by Hutchby and Fudurich in a theoretical modeling of graded-bandgap solar cells [ref. 1]. Our approach, which closely follows Maziar's, considers the contribution of all three band edges, $E_{\Gamma 1}$, E_L and E_{x1}, to the absorption process [ref. 2]. Equations for the value of the different bandgaps as a function of aluminum concentration were taken from Casey and Panish [ref. 3].

For direct transitions, the expressions for the absorption coefficients divide the absorption spectrum into three distinct regions: $h\nu \leq E_g$, $E_g \leq h\nu \leq E_g + \Delta_{so}$, and $h\nu \geq E_g + \Delta_{so}$ where Δ_{so} is the split-off band separation and taken as 0.33 eV. The first region follows an exponential equation and is known as the Urbach tail. We used an empirical relation with a two parameter fit as given in Maziar as

$$\alpha_\Gamma = B \exp[\gamma(h\nu - E_g^\Gamma)], \quad h\nu \leq E_g$$

with $B = 3000$ and $\gamma = 100$ as fit to GaAs data by Casey and Sells [ref. 4]. In the region $E_g \leq h\nu \leq E_g + \Delta_{so}$ the equation follows the form

$$\alpha_\Gamma = (A^\Gamma/h\nu)(h\nu - E_g^\Gamma)^{1/2}, A^\Gamma = 7.5 \times 10^4$$

Above the split-off band the absorption data is fit by the equation

$$\alpha_\Gamma = 3885(10^{0.543h\nu})(1 - x)$$

Again these equations are fit to data by Casey and Sells [ref. 5] which is also contained in Casey and Panish [ref. 3].

The indirect bandgap transitions give absorption data modeled by the following

$$\alpha = (B/h\nu)(h\nu - E_g)^2$$

for both the L and X bands with $B = 5.5 \times 10^4$ as given in Maziar [ref. 2].

Figure 5 shows the effect of the dead layer on calculated values of internal photoresponse. Note that as one increases the dead layer thickness, the curve essentially pivots about a center located on the "shoulder" of the curve ($\lambda \simeq 830$ nm). Values assumed for other parameters are:

$x = 0.65$
$L(F) = 5$ microns
$S(F) = 3 \times 10^4$ cm/sec
$L(B) = 5$ microns
$S(B) = 5 \times 10^3$ cm/sec

The most important assumption we had to make in order to fit the data was that $x = 0.65$, instead of 0.90. Figure 6 illustrates the sensitivity of the calculated photoresponse curves to the value of x.

Figure 7 depicts the effect of varying L(F) on the calculated curve. Note that the photoresponse curve between $\lambda = 350$ nm and $\lambda = 850$ nm shifts as L(F) is varied. Figure 8 shows the effect of varying S(F). The effects of L(F) and S(F) are very similar. As a result, we can only assign a range of values for these parameters. We estimate that L(F) is in the range of 2.0 to 5.0 microns, and S(F) is in the range of 10^4 to 3×10^4 cm/sec.

Figures 9 and 10 describe calculated internal response for ranges of L(B) and S(B), respectively. Like the parameters in the emitter region, the effects of L(B) and S(B) on calculated photoresponse curves are similar. We estimate the values for L(B) and S(B) to be 4.0 to 6.0 microns and 10^3 to 5×10^3 cm/sec., respectively. Results of the photoresponse analyses are summarized in Table 2.

Results of the photoresponse analyses have been used to determine potential increases in photocurrent. Table 3 summarizes key results of the photon economy analysis. Values of photocurrent were calculated by integrating internal photoresponse data (or calculated curves) over the solar spectrum. In particular, J_{PH} is calculated by

$$J_{PH} = \int_{\substack{\text{Solar} \\ \text{Spectrum}}} q\, N_\lambda\, S_\lambda\, d\lambda$$

where N_λ is the photon flux with wavelengths in the interval λ to $\lambda + d\lambda$. We find that the maximum possible value for J_{sc} is 31.6 mA/cm^2. The measured active current was 25.7 mA/cm^2. If we assume the AlGaAs window layer has an aluminum concentration of $x = 0.9$, then the active area current should increase to 26.9 mA/cm^2. If the dead layer were eliminated, then an increase of 0.8 mA/cm^2 would be obtained. A double AR coating would subsequently increase $(J_{sc})_{ACTIVE}$ to 29.0 mA/cm^2. Such a value for $(J_{sc})_{ACTIVE}$ is approximately the same as that reported by Spire Corporation. If we assume the collector grid shadowing to be 3%, $V_{oc} = 1.016$ Volts, FF = 85.1%, then an efficiency of 24.3% would be achieved.

T–I–V Analyses

Current-voltage data have been taken for various temperatures from -30 C to 60 C, and then analyzed in terms of accepted theoretical models. I-V data at a particular temperature can usually be interpreted in terms of two current mechanisms acting in parallel. One mechanism is dominant at low voltages (0.4 to 0 8 Volts), and another is dominant at higher voltages (0.8 to 1.1 Volts). The upper mechanism is usually characterized by an n-value of 1.0 and $J_0 = 3 \times 10^{-19}$ A/cm^2, and can be interpreted as being due to minority carrier injection. The lower mechanism of the 21% to 22% cells is characterized by an n-value of approximately 2.0. Thus, we can interpret these characteristics as being due to depletion region recombination.

J_0-T analyses have also been carried out. We assume J_0 can be written as

$$J_0 = J_{00}\exp(-\phi/kT)$$

$\phi = E_{g0}$, Minority Carrier Injection

$\phi = E_{g0}/2$, Depletion Region Recombination

where $E_g = E_{g0} - aT$.

J_0-T analyses involve plotting Log(J_0) versus T^{-1} so that J_{00} and ϕ can be determined. Figure 12 shows Log(J_0) versus T^{-1} for the large voltage mechanism (A), and the low voltage mechanism (B). The activation energies, ϕ = 1.50 eV and 0.68 eV are consistent with minority carrier injection and depletion region recombination, respectively.

Conclusions

Photocurrent analyses of 21 to 22% GaAs cells indicate that an improved AlGaAs/GaAs interface in the emitter region, and a double AR coating will lead to an active area, AM1 value for J_{sc} of 29 mA/cm^2. This result combined with properties of cells reported in this paper would yield cells with total area, AM1 efficiencies greater than 24%. Further reduction of the magnitude of the depletion-layer-recombination current mechanism will allow efficiencies to exceed 25%. A new MOCVD reactor will be operational at TUC July, 1988. We plan to concentrate on improving the front surface AlGaAs/GaAs interface to obtain larger values of J_{sc}; and continue to improve edge passivation procedures in order to reduce the depletion layer recombination mechanism, which will lead to larger values of FF and V_{oc}.

References

[1] James A. Hutchby and Richard L. Furdurich, "Theoretical Optimization and Parametric Study of n-on p-$Al_xGa_{1-x}GaAs$ Graded Band-Gap Solar Cells" Journal of Applied Physics **47**, 3152-3158 (1976).

[2] Maziar MS Thesis, Purdue University, 1984.

[3] H.C. Casey, Panish, *Heterojunction Lasers, Part A*, Academic Press, 1978.

[4] H.C. Casey, D.D. Sell and K.W. Wecht, "Concentration Dependence of the Absorption Coefficient for n- and p-type GaAs Between 1.3 and 1.6 eV," Journal of Applied Physics **46**, 250-257 (1975).

[5] D.D. Sell, H.C. Casey and K.W. Wecht, "Concentration Dependence of the Absorption Coefficient for n- and p-type GaAs Between 1.3 and 1.8 eV," Journal of Applied Physics **45** 2650-2657 (1974).

Table 1. Cell Fabrication Procedure

1. Grow Layered Structure by MOCVD (by Spire Corporation).
2. Dice Wafer into 1.5 X 1.5 cm Die.
3. Clean Die.
4. Apply and Pattern Photoresist.
5. Electroplate Au Collector Grid on P-Type Emitter.
6. Electroplate Au(Sn) on N-Type Substrate for Back Contact.
7. Heat Treat Contacts.
8. Form Mesa Junction.
9. Etch GaAs Cap.
10. Apply SiN_x AR Film.

Table 2. Results of Photoresponse Analyses

Apparent $Al_xGa_{1-x}As$ Composition:	x = 0.65
Dead Layer in GaAs:	40Å to 60Å
Emitter Parameters:	
	S(E) = 1E4 - 3E4 cm/sec
	L(E) = 2.0 - 5.0 microns
Base Parameters:	
	S(B) = 1E3 - 5E3 cm/sec
	L(B) = 4.0 - 6.0 microns

Table 3. AM1 Photocurrent of GaAs Cells

	Active Area Current (mA/cm^2)
Maximum J_{sc}	31.6
Measured Active Area J_{sc}	25.7
TUC Cell with $Al_xGa_{1-x}As$ Window Layer, $x = 0.90$	26.9
TUC Cell with No Dead Layer	27.7
TUC Cell with No Dead Layer and DBL AR	29.0

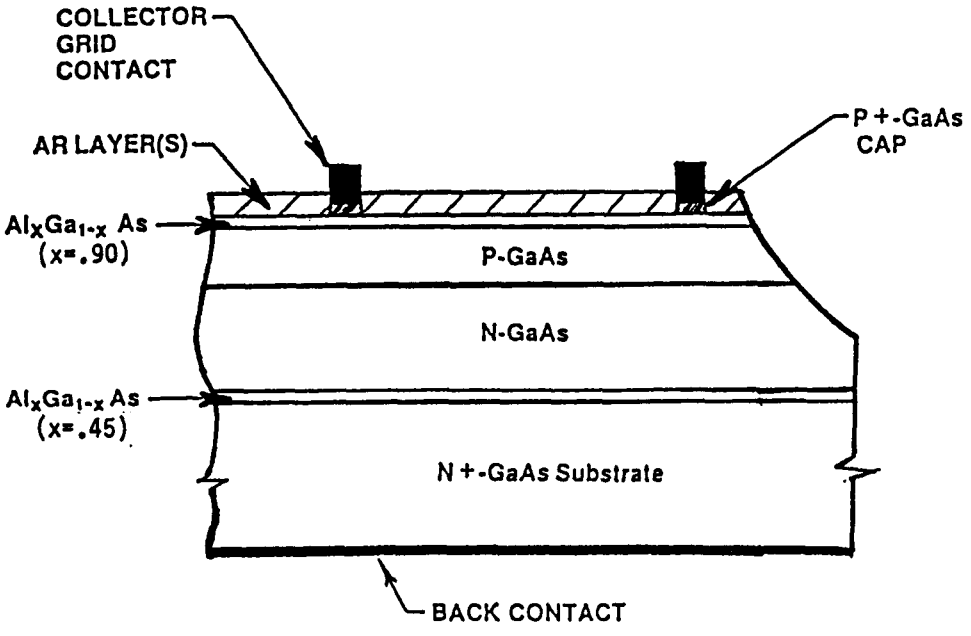

LAYER	ALUMINUM CONCENTRATION (%)	DOPANT CONCENTRATION (cm^{-3})	THICKNESS (μm)
P^+ GaAs CAP	-	Zn: >3E18	0.1
P-AlGaAs WINDOW	90%	Zn: 1E18	.05
P-GaAs EMITTER	-	Zn: 1E18	0.5
N-GaAs BASE	-	Si: 3E17	3.0
N-AlGaAs REFLECTOR	45%	Si: 1E18	0.1
N-GaAs BUFFER	-	Si: 1E18	0.5
N-GaAs SUBSTRATE	-	Si: >1E18	-

Figure 1. GaAs Cell Structure.

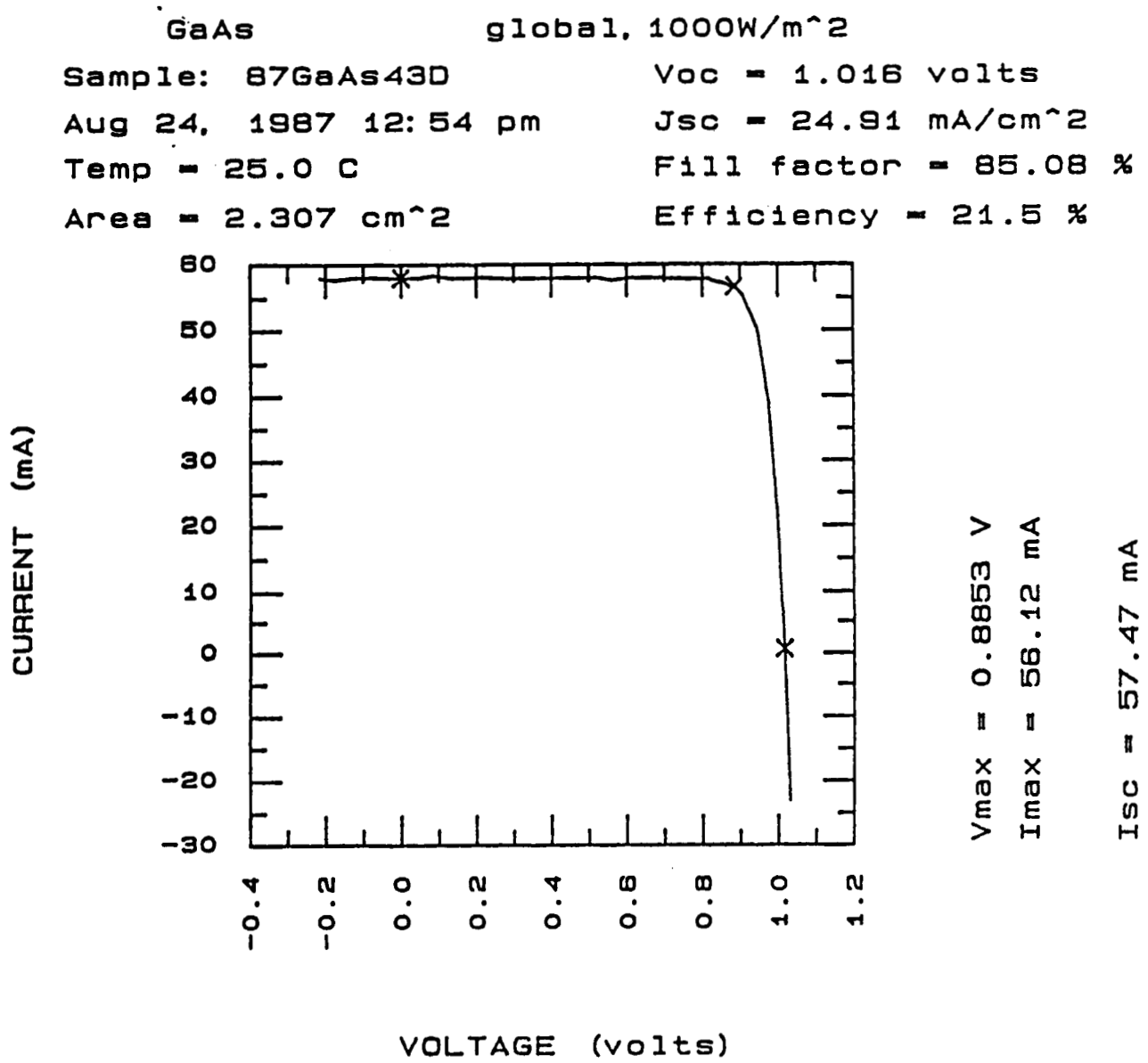

Figure 2. Illuminated I-V Characteristics for a GaAs Cell Measured by SERI.

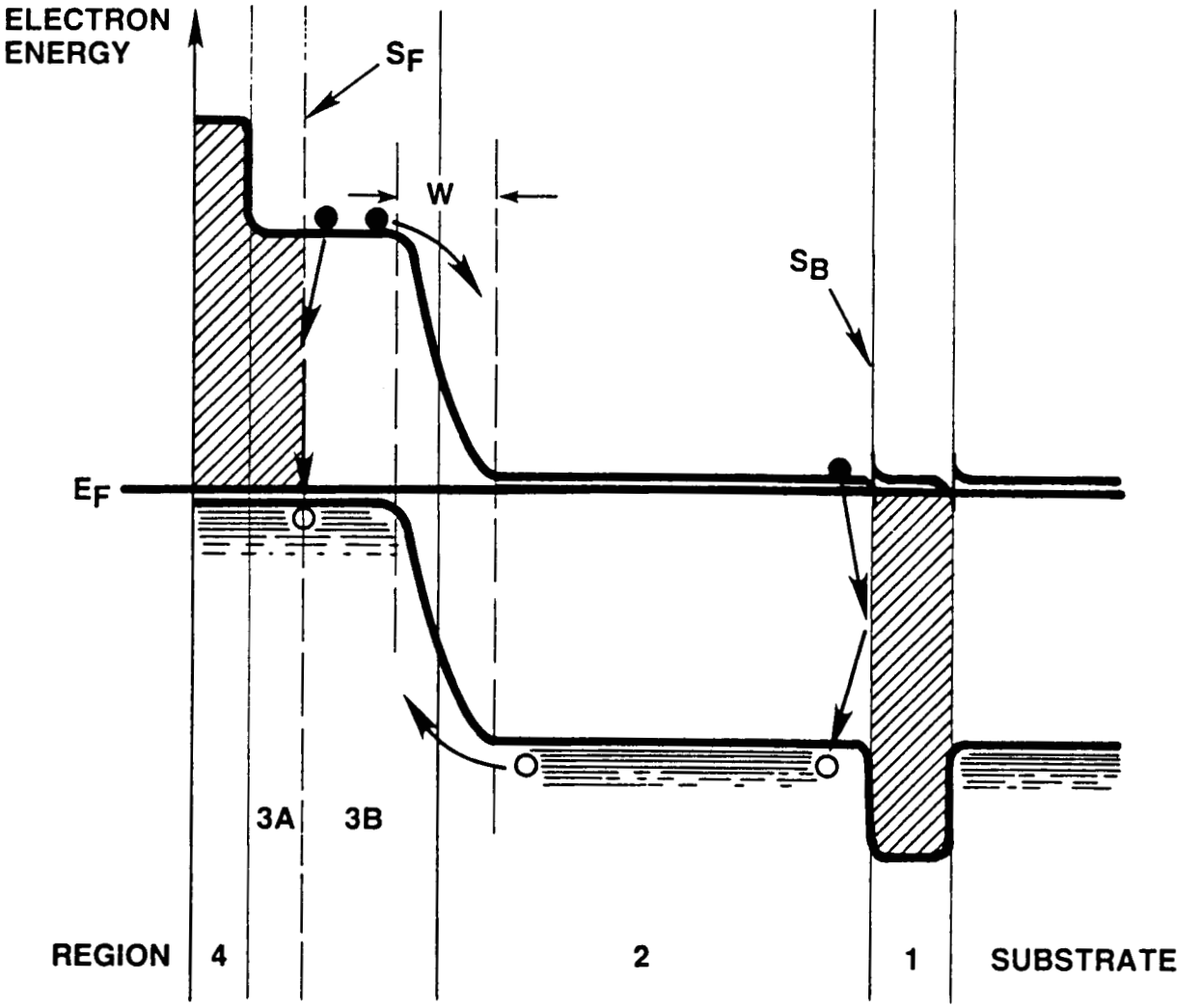

Figure 3. Assumed Electron Band Structure for GaAs Cells.

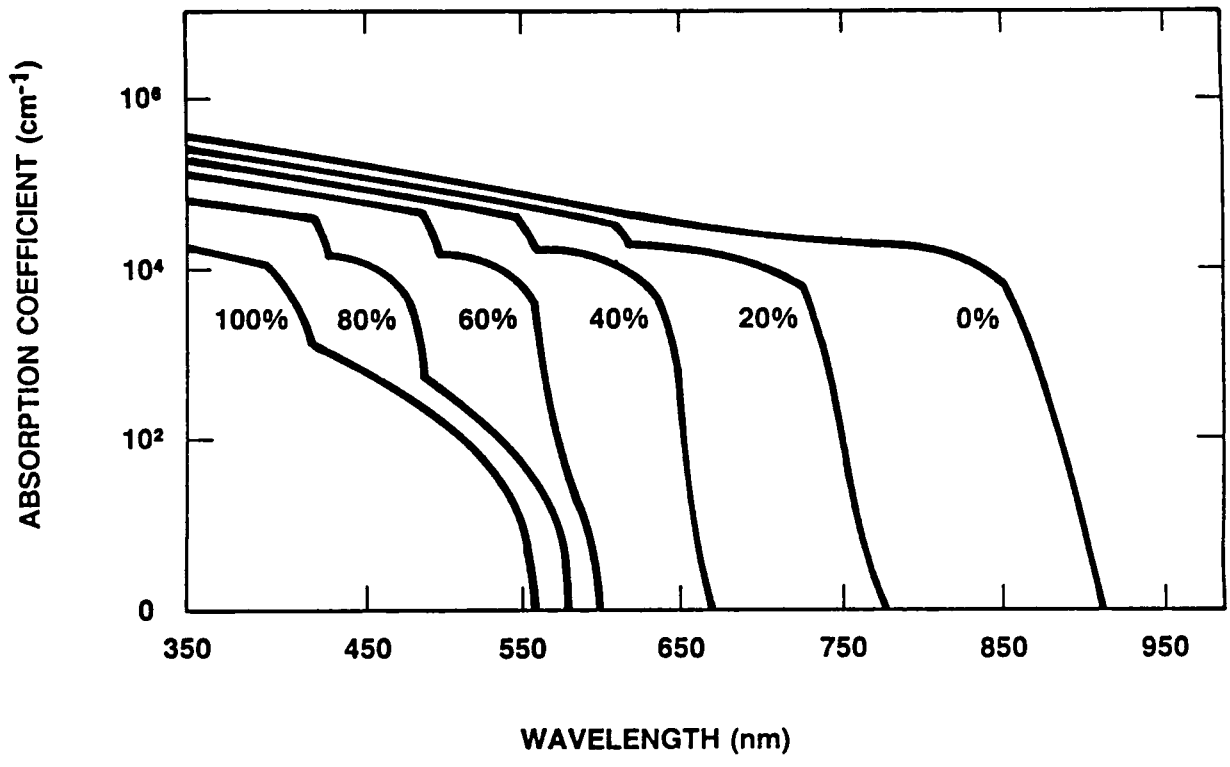

Figure 4. Al_xGa_{1-x} As Optical Absorption Coefficient for Various Values of x.

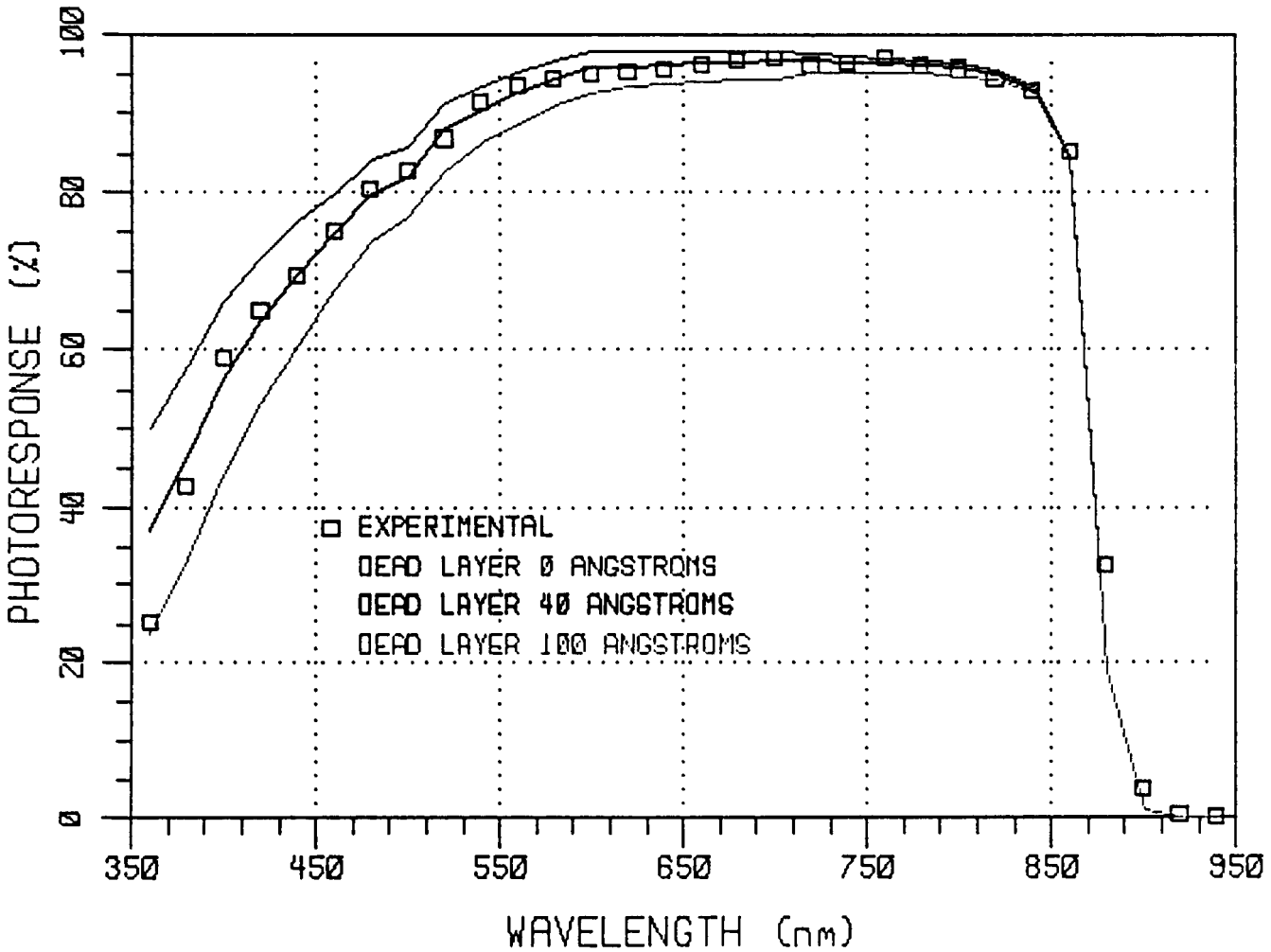

Figure 5. Experimental Data and Calculated Values for Internal Photoresponse versus Wavelength for Three Dead Layer Thicknesses.

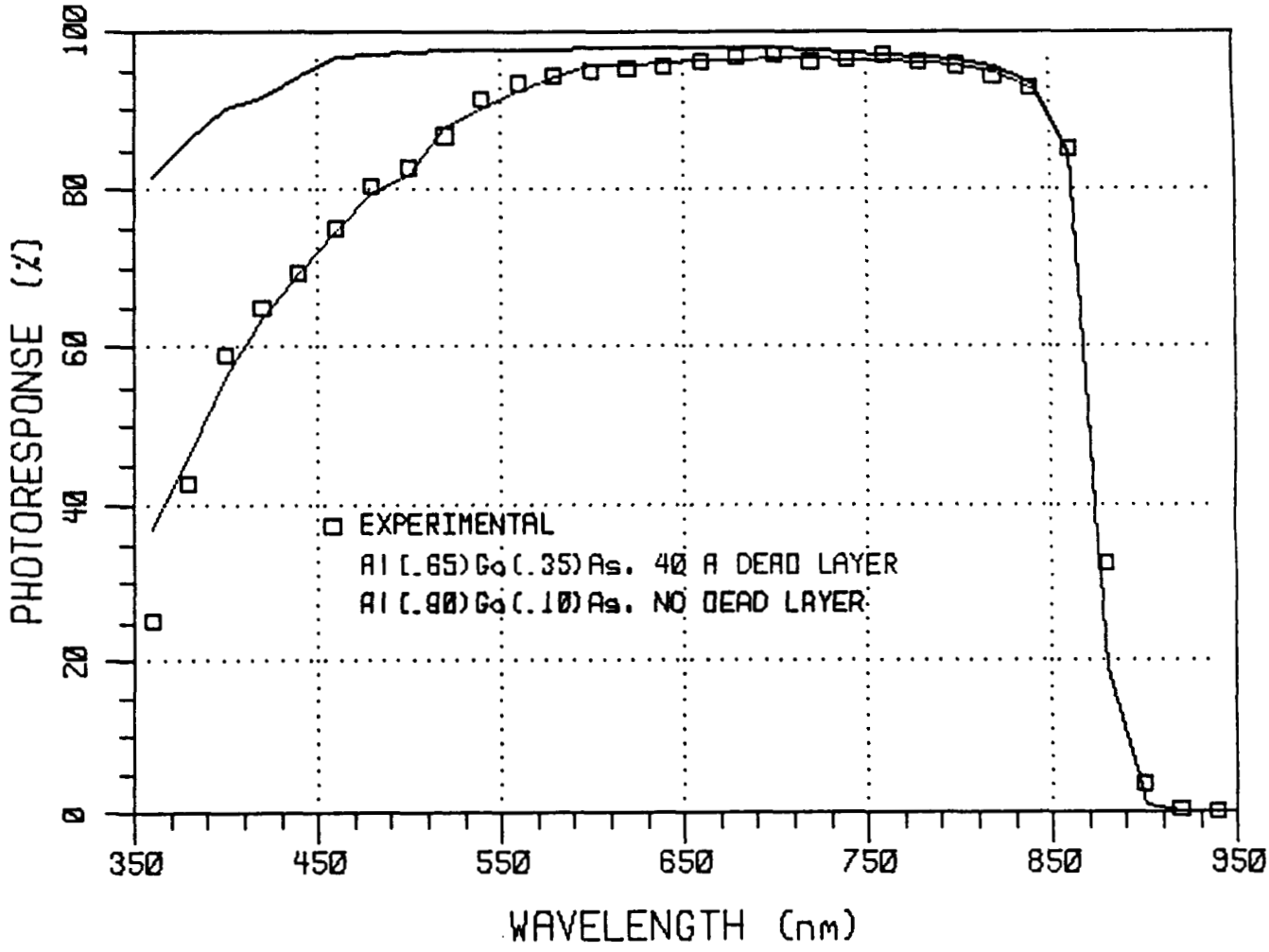

Figure 6. Experimental Data and Calculated Values for Internal Photoresponse Assuming x = 0.9 and No Dead Layer, and x = 0.65 and a Dead Layer Thickness of 40 A.

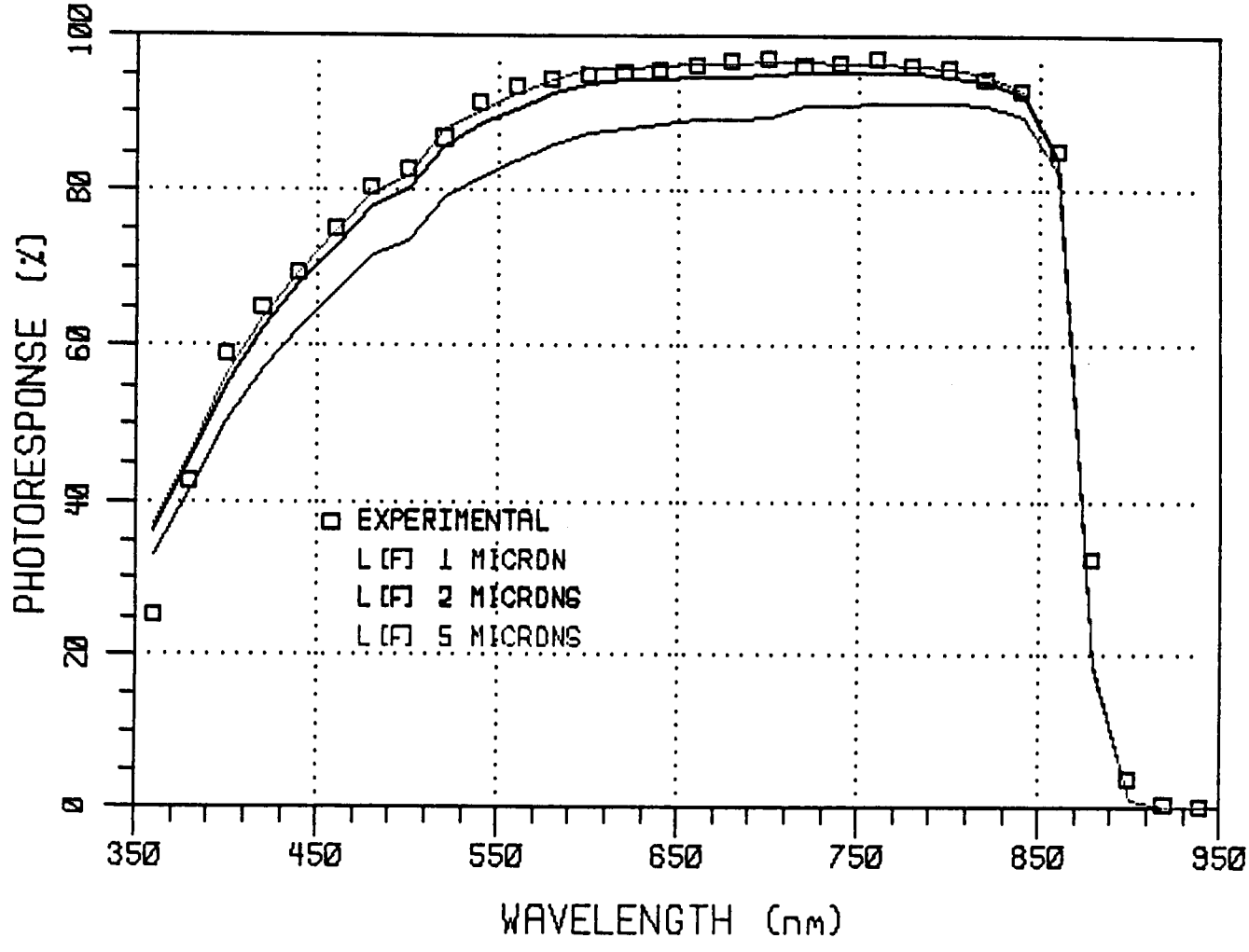

Figure 7. Calculated Values of Internal Photoresponse for a Range of Values for the Emitter Diffusion Length, L(F).

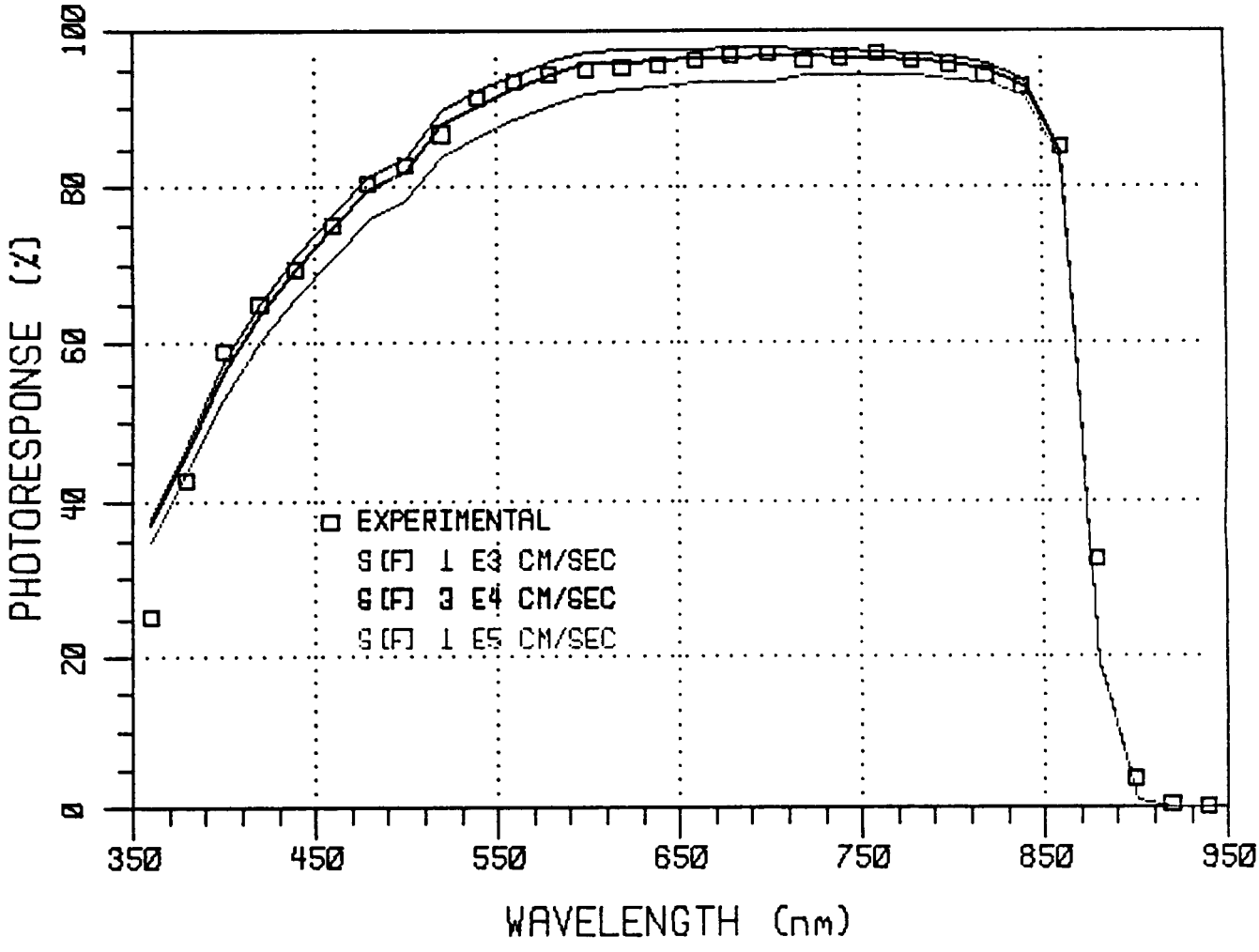

Figure 8. Calculated Values of Internal Photoresponse for a Range of Values for the Emitter Surface Recombination Velocity, S(F).

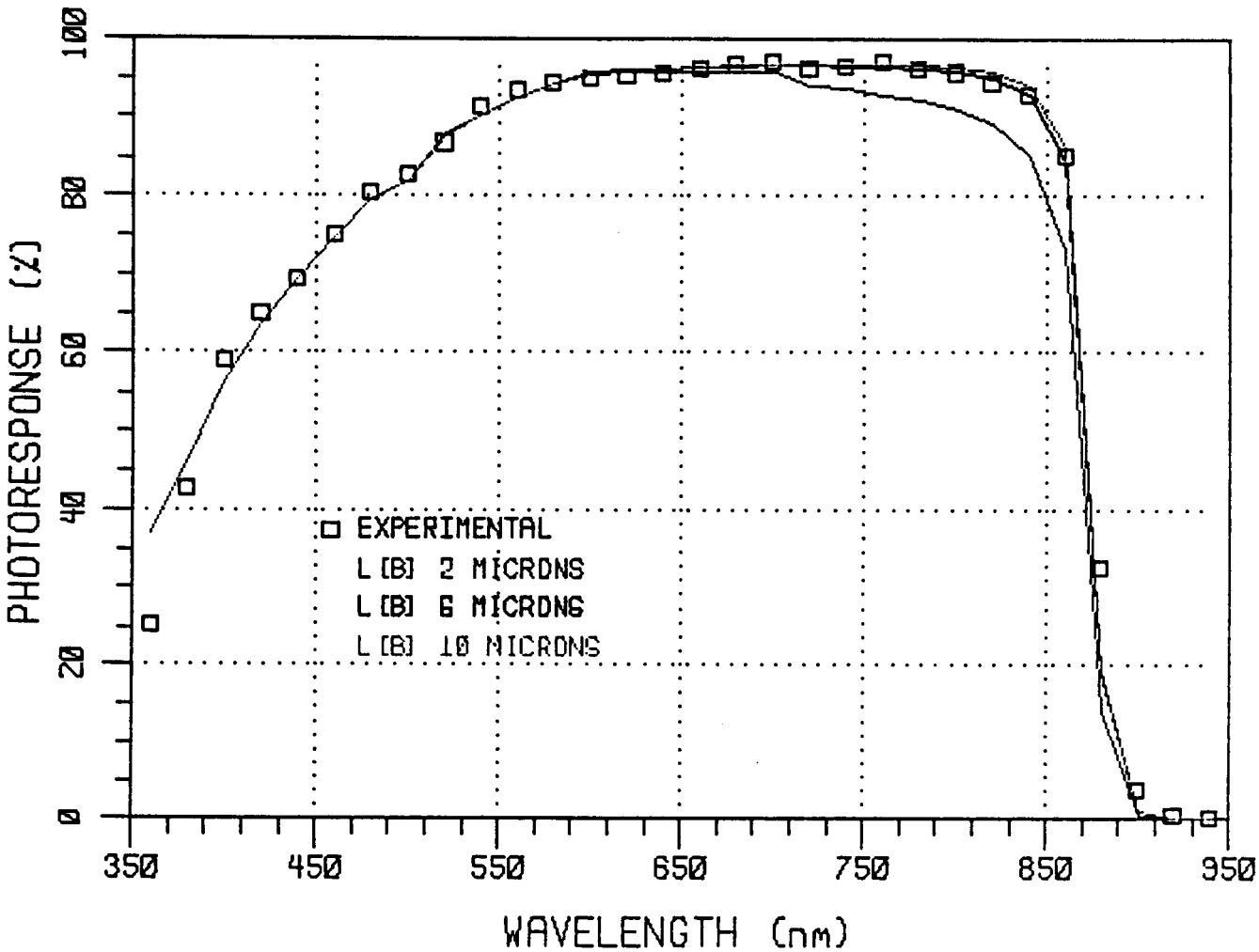

Figure 9. Calculated Values of Internal Photoresponse for a Range of Values for the Base Diffusion Length, L(B).

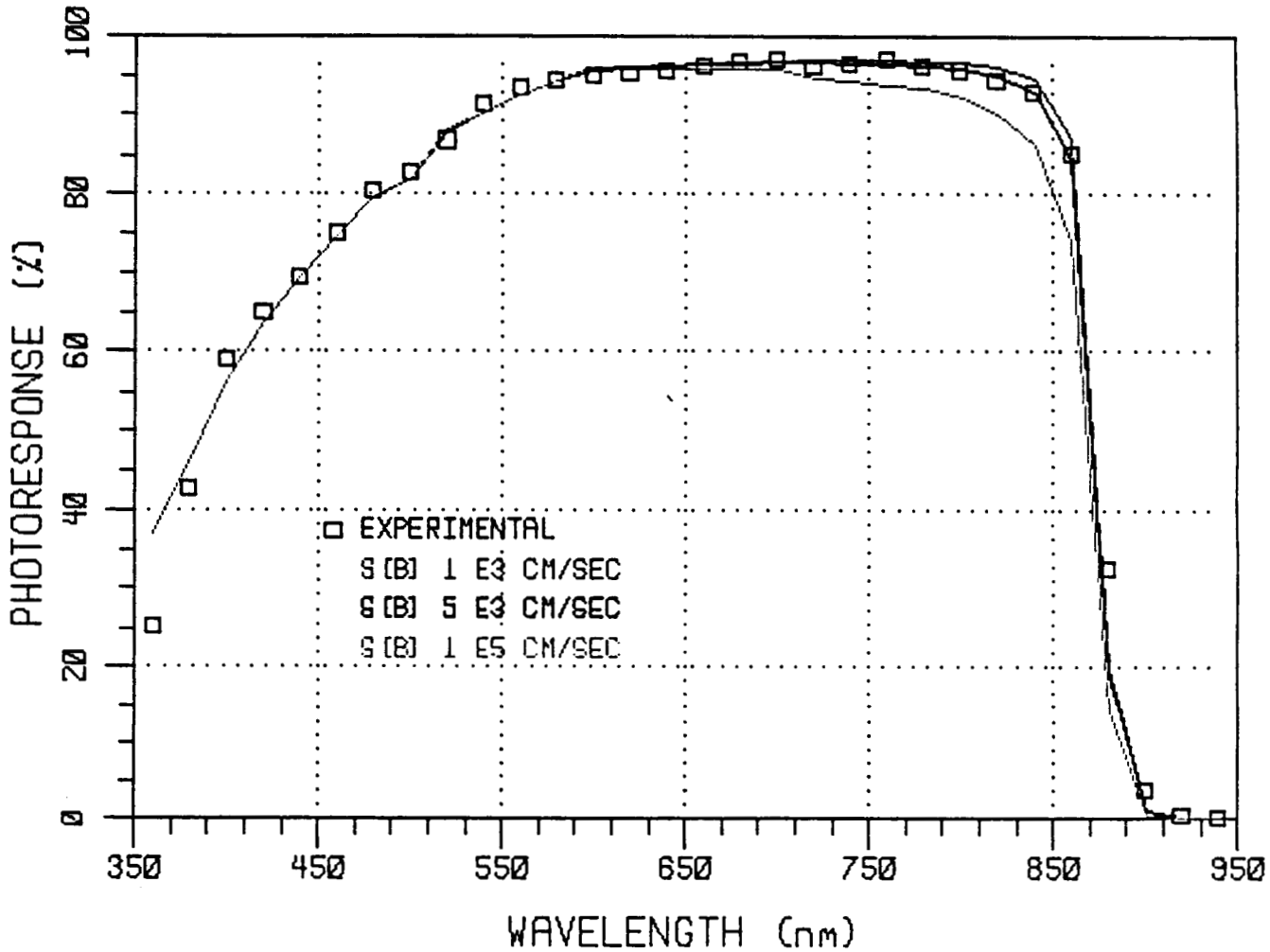

Figure 10. Calculated Values of Internal Photoresponse for a Range of Values for the Surface Recombination Velocity at the Back Surface, S(B).

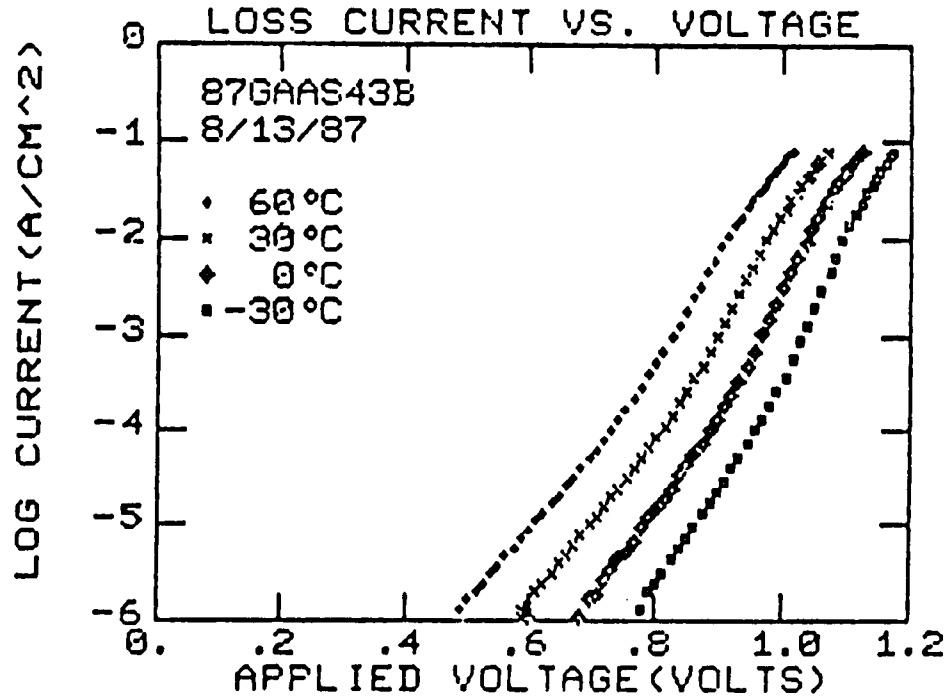

Figure 11. I-V Data Measured for Various Temperatures.

(A)

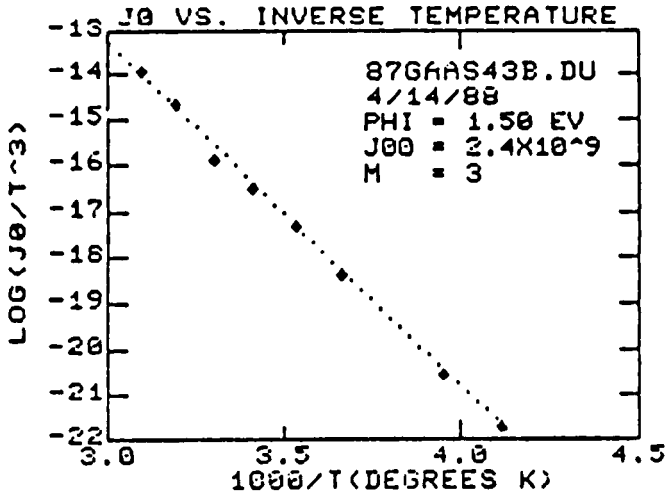

(B)

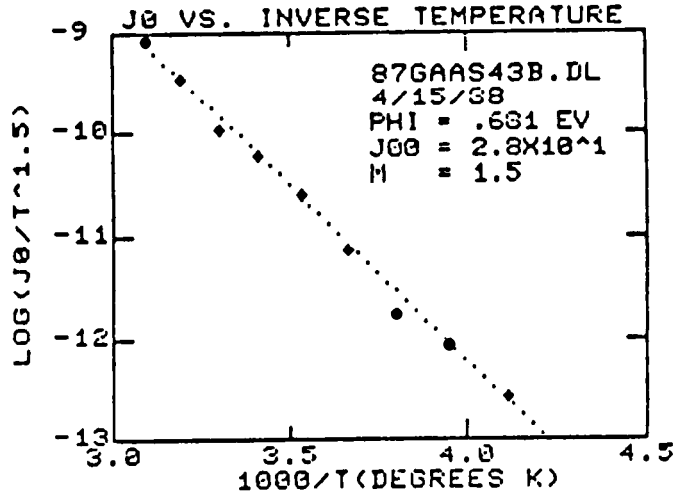

Figure 12. J_o-T Analysis for GaAs Cell 87-43. (A) Log J_o versus T^{-1} for the Large Voltage Mechanism. (B) Log J_o versus T^{-1} for the Low Voltage Mechanism.